CONJUNCTION ASSESSMENT FOR COMMERCIAL SATELLITE CONSTELLATIONS USING COMMERCIAL RADAR DATA SOURCES

Michael Nicolls*[1], Vivek Vittaldev†[2], Dan Ceperley[1], Joan Creus-Costa[2], Cyrus Foster[2], Nathan Griffith[1], Ed Lu[1], James Mason[2], In-Kwan Park[1], Chris Rosner[1], and Leon Stepan[2]

[1]*LeoLabs, Inc., PO Box 998, Menlo Park, CA 94026-0998*
[2]*Planet Labs, Inc., 346 9th Street, San Francisco, CA 94103*

September 12, 2017

ABSTRACT

For companies with multiple orbital assets, managing the risk of collision with other low-Earth orbit (LEO) Resident Space Objects (RSOs) can amount to a significant operational burden. LeoLabs and Planet investigate the impact of a workflow that integrates commercial Space Situational Awareness (SSA) data into conjunction assessments for large satellite constellations.

Radar measurements from LeoLabs are validated against truth orbits provided by the International Laser Ranging Service (ILRS) and to measurements from Planet's on-board GPS instrumentation. The radar data is then used as input for orbit fits in order to form the basis of a conjunction assessment. To confirm the reliability of the orbit determination (OD), the generated ephemerides are validated against ILRS and GPS-derived orbits. In addition, a covariance realism assessment is performed in order to check for self-consistency by comparing the propagated orbit and the associated covariance against later measurements.

Several cases are investigated to assess the benefits of integrating radar-derived products with Conjunction Data Messages (CDMs) received on Planet spacecraft. Conjunction assessment is refined using onboard GPS measurements from Planet satellites along with tracking measurements of the secondary RSO by LeoLabs. This study demonstrates that commercial data provided by LeoLabs is reliable, accurate, and timely, and that ephemeris generated from LeoLabs data provides solutions and insights which are consistent with those provided in CDMs. For the cases analyzed, the addition of commercial SSA data from LeoLabs has a positive impact on operations due to the additional information on the state of the secondary RSO which can lead to increased confidence in any maneuver-related decisions. Measurements from LeoLabs can also be used to improve conjunction assessment for commercial satellites that do not have any operator OD.

1. INTRODUCTION

The number of active satellites in low-Earth orbit (LEO) has increased rapidly over the last few years, and this growth is accelerating. Global imaging, internet-of-things backhaul, and broadband internet access are only a few of the services being built in LEO that are becoming critical for commercial, civilian, and defense organizations. This growth has also driven the rise of a range of supporting services such as new low-cost launch opportunities, global ground-station networks, and off-the-shelf spacecraft and component solutions. Taken in total LEO is maturing into an area of significant economic opportunity.

With this growth comes a need for services to support safe and reliable operations. Satellite operators need commercial tracking and navigation services that will enable them to continue to increase their use of LEO in a sustainable and safe manner. One of the primary concerns is the risk of collision with debris. Collision-avoidance services must provide actionable data and be fully automated so that large constellations can operate efficiently. As LEO becomes more heavily used the risk of collision increases. This risk is dominated by the large amount of small, untracked debris. At present, the risk of collision with an object 1 cm or larger peaks at about 750 km altitude with a probability of about 10^{-3}/year for a 2 m^2 satellite. This number is no longer vanishingly small - with over 800 active

*mike@leolabs.space
†vivek@planet.com

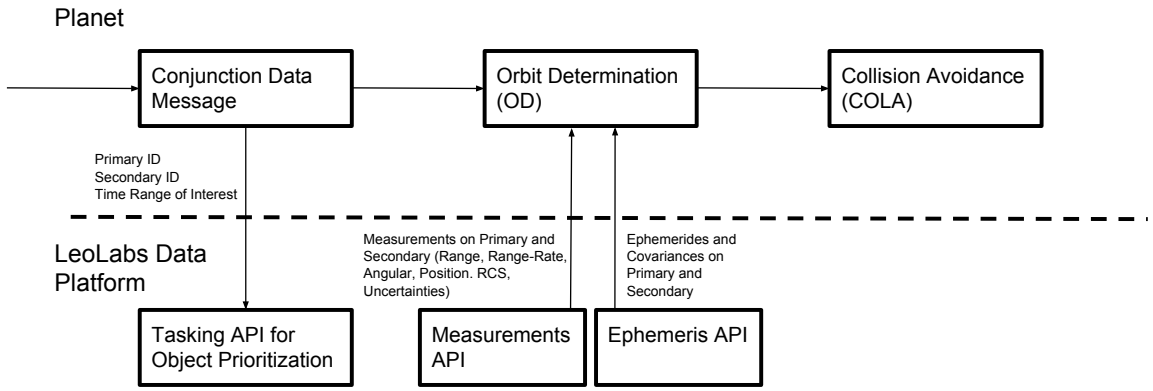

Figure 1: Data flow diagram for Planet CDM processing with the addition of LeoLabs' commercial data.

satellites in LEO, this portends a catastrophic collision every year. In addition, the number of operational satellites in LEO is projected to increase from hundreds to thousands or even tens of thousands over the coming decades. New constellations plan to replace satellites every $\sim$5 years to leverage low-cost satellite technologies, utilize low-cost launch vehicles, and refresh their on-orbit technology frequently, which means that a significant number of satellites will be undergoing orbit raising and lowering operations through populated orbits.

In this paper, LeoLabs and Planet present a workflow that integrates commercial space situational awareness (SSA) data into conjunction assessments and demonstrate the workflow with the Planet constellation of cubesats. The results, and the lessons learned during development and implementation, can be utilized by other LEO operators. Eventually, the intention would be to integrate this workflow into automated flight systems.

A notional workflow for the ingestion of external data sources is shown in Fig. 1. The process begins with the handling of conjunction data messages (CDMs), typically issued by the US Air Force's Joint Space Operations Center (JSpOC). Included in a CDM is information on an upcoming conjunction, including the catalog identifiers for the primary and secondary, state and covariance information, miss distance, the time of closest approach (TCA), and sometimes a probability of collision (P_c). A typical workflow would use the information contained in the CDM, and its evolution with time, to assess the need to make a collision avoidance maneuver and the details of that maneuver.

The addition of external data from commercial data sources such as LeoLabs can help refine the conjunction parameters in order to allow operators to discard the unimportant conjunctions earlier and highlight the ones of high risk. This refinement is accomplished primarily by improving the state estimates of the secondary object through the use of additional data. The interaction can come as soon as a CDM is received. LeoLabs is currently tracking most objects in the public JSpOC catalog; however, it can prioritize collections of objects of high interest. A first step is to access the historical data available in LeoLabs' archive and request priority tracking status on the secondary object so that additional measurements can be collected in the days leading up to TCA. A second step is to fuse the radar measurements to form an ephemeris that can be used for additional screening. In this way there are several data combinations that can be used to compute conjunction parameters, including:

Data Source for Primary	Data Source for Secondary
CDM	CDM
Planet	CDM
Planet	LeoLabs
LeoLabs	LeoLabs

While typically the owner-operator data on the primary is more accurate than the ephemeris generated from external tracking, the additional ephemeris and covariance on the secondary can significantly increase confidence in the conjunction-parameter estimates. In cases when the parameters using different data-source combinations agree, there can be high confidence in the accuracy of the results. In cases when they disagree, additional investigation of the errors from each source needs to be made. In this paper we investigate multiple cases to assess the benefits of integrating radar-derived products with CDMs received on Planet spacecraft.

2. PLANET SATELLITE CONSTELLATION

2.1. OVERVIEW

Planet Labs Inc. (also referred to as simply Planet) is a space and data analytics company headquartered in San Francisco, California. The company designs, builds and operates large fleets of Earth-observation small satellites to image the entire planet at an unprecedented frequency. Planet aims to provide universal access to information about the changing world to enable both commercial and humanitarian applications.

Planet operates three classes of satellites: 5 RapidEye satellites with 5-m resolution in a 600-km orbit, 7 Skysats with $<$1-m resolution mostly in a 500-km orbit, and 192 Dove satellites with 4-m resolution also mostly in a 500-km orbit. This paper will focus on the Dove satellites as a use-case; a treatment of collision avoidance operations on the Skysats, which have propulsion, can be found in [5].

Planet's Dove satellites (Fig. 2) are roughly 30x10x10 cm in dimension (3U cubesat form factor) and are equipped with an Earth-imaging telescope, 3-axis attitude-control system, a high-speed X-band radio, and a large deployed solar panel enabling them to make substantial differential-drag maneuvers [4]. The satellites are deployed and maneuvered into constellations where their overlapping swaths provide near-daily coverage of the planet at $\sim$4-m resolution.

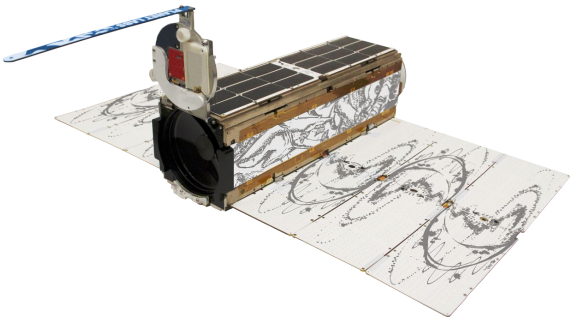

Figure 2: Dove Satellite

2.2. OPERATIONS

Planet's concept of operations differs fundamentally from other satellite operators. The scale of the fleet ($\sim$200 satellites) precipitated the need for a complete automation of operations for scheduling satellite and ground-station activities, imaging, and fault detection. A small team of operators spend their time monitoring these automated operations, running experiments, or troubleshooting new issues.

Two types of orbit knowledge data are acquired from the Doves [3]:

- *Ranging*: Two-way time-of-flight ranging data is acquired over UHF radio, where packets are tagged with the serial number of the satellite to be interrogated, ensuring positive identification and eliminating the possibility of cross-tagging. Given Planet's worldwide network of UHF ground stations and the wide field-of-view of their antennas, ranging is low-latency but provides a medium accuracy orbit data product ($\sigma \approx 600$ m, range-only).
- *GPS*: The Dove satellites are also equipped with software-defined GPS units and navigation data is downloaded at every X-band contact opportunity. They provide a higher latency but far more accurate ($\sim$10-m position) source of position/velocity/time measurements.

For OD, acquired ranging and GPS data are fit to a high-precision propagator model using a non-linear least-squares solver. The propagator numerically integrates state vectors using the EGM96 spherical-harmonic gravity field [8] and the NRLMSISE-00 atmosphere model [13] updated with latest space-weather data from NOAA. Data products from OD include state vectors, TLEs fit to the numerical propagator, and 10-day ephemeris predictions. Differential-drag maneuver planning is performed by a ground-based controller which ingests state vectors from the OD and outputs schedules of high-drag maneuvers for every satellite. Fig. 3 shows a high-level systems diagram from this fully automated OD and control process.

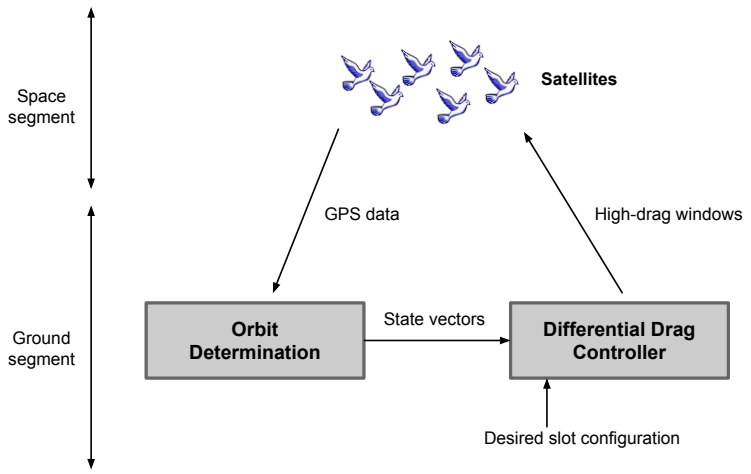

Figure 3: Automated Planet OD and differential drag loop

2.3. CONJUNCTION STRATEGY

Planet cares deeply about operating openly and responsibly in space to ensure sustainable and universal access to LEO. Since Planet's first launch, it has strived to reach this goal with the following three-pronged strategy:

Launch Low: Selecting orbits that have low altitudes is the single biggest factor for reducing Planet's impact on the space environment. Launching low reduces the time spent in orbit and ensures that Doves are flying below the congested 700-1000-km orbital band. In the unfortunate event of a collision, debris fragments will also have a short lifetime, further reducing the negative impact. Planet's model of many small, relatively cheap, and short-lived satellites allows launching into orbits with lifetimes of a few years ($\sim$500-km altitude), as opposed to larger satellites that prefer to maximize time in orbit. Planet always ensures that their satellites are well below the United Nations' 25-year guideline, and will never launch a satellite into an orbit with a predicted lifetime greater than 25 years.

Open Orbit Data: TLE-derived orbits are not accurate enough for collision avoidance. To help increase the accuracy of collision predictions Planet maintains a public orbit catalog for its own satellites, which is automatically updated on an hourly basis[1]. Planet is a member of the Space Data Association (SDA), which streamlines the delivery of orbit solutions to other operators. Planet also reports all launches and orbits to JSpOC, and publicly shares matching reports between GPS-derived orbits and space-track.org TLEs.

Conjunction Response: It is inevitable over time that high-risk conjunctions will occur, and if the risk is deemed unacceptable preventative actions become necessary. The Dove satellites are not equipped with propulsion, so avoidance options are limited. For all conjunctions with active, maneuverable satellites, operators are contacted and directed towards Planet's latest ephemeris predictions. If the conjunction is with any other object and has a small miss distance (and similarly small uncertainties), the Doves are commanded into a minimum interaction-area attitude configuration at the TCA. Planet is also actively investigating and implementing the use of differential drag for performing conjunction avoidance maneuvers. The effectiveness of such a maneuver is a function of lead-time, atmospheric density, and state-vector covariances, and its treatment will be left to a subsequent paper.

2.4. DOVE ORBIT-DETERMINATION PERFORMANCE

On-board GPS measurements are used for orbit determination on most Doves. GPS measurements are periodically collected when the Dove is imaging or downlinking, resulting in samples on an hourly cadence. GPS samples are downloaded during a Dove's ground-station pass and an orbit is fit on the ground. Estimation involves a batch least-squares (BLS) fit using approximately 18 hours of GPS samples. Note this long-term OD is used in production and differs from the short term OD used to assess LeoLabs measurements in Sec. 4.4.

Conjunction assessment requires predictions of the state and associated uncertainty. The OD state at epoch is numerically integrated to generate the state prediction. Polynomial fits for the uncertainty for flocks of satellites in roughly the same orbit are used to compute the uncertainty of the state prediction. Given an orbital fit at some past epoch,

[1] `http://ephemerides.planet-labs.com/`

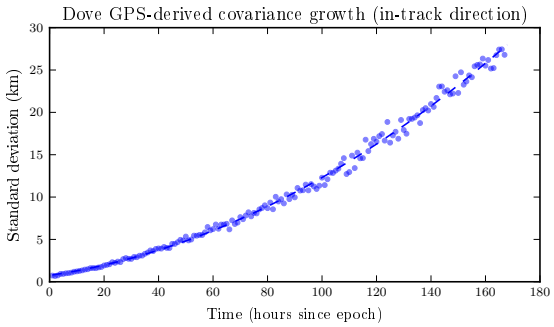

Figure 4: Uncertainty growth over time for Planet's Flock 2p satellites.

the states are propagated forward in time and the error is measured against GPS measurements, which are assumed to be the truth. By performing this test on a large sample of $(\text{satellite}, \text{time})$ pairs (in this case, about a thousand) and binning the residuals in the radial, in-track, cross-track (RIC) reference frame by the number of hours since the fit epoch, an estimate of the covariance growth over time can be derived. Fig. 4 shows the standard deviation growth in the in-track direction given an orbital fit derived from GPS measurements. The uncertainty in the radial and cross-track directions are roughly constant with a standard deviation of 100 m. The growing standard deviation in the in-track direction with units in meters is given by

$$\sigma_I(t) = 6.8 \times 10^{-4} \cdot \Delta t^2 + 0.047 \cdot \Delta t + 0.75 \tag{1}$$

where Δt is the time in seconds since OD epoch,

$$\Delta t = \min(0, t - t_{OD}). \tag{2}$$

The position uncertainty in the RIC reference frame of a Dove therefore, has the following covariance matrix:

$$\mathbf{P}_{RIC}(t) = \begin{bmatrix} 100^2 & 0 & 0 \\ 0 & \sigma_I^2(t) & 0 \\ 0 & 0 & 100^2 \end{bmatrix}. \tag{3}$$

3. LEOLABS

3.1. LEOLABS RADAR NETWORK

LeoLabs was founded to be a commercial provider of high-performance tracking and mapping data for LEO. This data will power a broad range of applications such as protecting satellites from collisions and informing best practices in LEO; tracking satellites immediately after deployment to guide them through early operations; troubleshooting malfunctioning satellites by determining if they are tumbling, in a new orbit, or intact; and enabling accurate modeling of on-orbit risks. LeoLabs is designed to be the data layer of the software stack for LEO and this data will support and empower a new wave of application developers bringing new services to market.

LeoLabs is a startup that spun out of SRI International (SRI), a not-for-profit research lab, in mid-2016. The founding team includes principal engineers and scientists from the radar program at SRI and a NASA astronaut who is actively involved in protecting the Earth from Near Earth Objects (NEOs). The radar technology used by LeoLabs has operated successfully for over a decade in the harsh arctic environment as the Poker Flat Incoherent Scatter Radar (PFISR). This radar has demonstrated high fidelity tracking of objects in LEO for several years [10, 11]. In February 2017, LeoLabs completed the Midland Space Radar (MSR), the second radar in its global network (see Fig. 5). LeoLabs' radars are phased arrays, with no moving parts and the ability to track more than 1,000 objects per hour. This high tracking rate is critical for persistently monitoring and avoiding the entire population of space debris. The field-of-view (FOV) of the two radars is depicted in Fig. 6. PFISR, a two-dimensional phased array, has a star-shaped FOV. MSR is a one-dimensional phased array. Both radars operate in the UHF band, 430-450 MHz, and have the ability to detect objects 10 cm and larger in LEO. PFISR, with its much higher peak power, has more sensitivity to smaller objects and to objects at higher altitudes. See Table 1 for details on the two systems.

Figure 5: The Midland Space Radar (MSR).

Radar	Location	Latitude	Longitude	Peak Power	System Gain
PFISR	Fairbanks, Alaska	65.13°N	147.47°W	1.3 MW	41 dBi
MSR	Midland, Texas	31.96°N	103.23°W	65 kW	39 dBi

Table 1: LeoLabs' contributing radars.

When fully built out, LeoLabs' radar network will deliver the following capabilities which are critical for protecting satellites from debris:

1. *Rapid revisits* - revisits on most objects every few hours, leading to accurate ephemerides, prompt detection of new debris, and rapid tracking of newly launched satellites;
2. *Accuracy and precision* - range residuals of better than 15 meters, leading to ephemerides with uncertainties of 10s to 100s of meters (see Sec. 4);
3. *Full coverage* - measurements of RSOs in all inclinations and up to 2000 km altitude;
4. *Small debris data* - tracking data on objects as small as a few cm (estimated to be several hundred thousand objects).

Today LeoLabs' two radars have visibility to more than 95% of the public catalog in LEO. These radars track objects at inclinations of 30° and higher, and objects that are 10 cm in size and larger. They are typically able to revisit these objects between 1 and 3 times per day when prioritized. In 2018 and 2019, LeoLabs will build 4 more radars, located near the equator and near the poles, that will increase the revisit rate and detect smaller debris.

3.2. LEOLABS' DATA PLATFORM

The data platform is LeoLabs' interface to the space community. The platform provides customers access to data services, including real-time tracking data from the radars, calibration and validation data, schedules for upcoming measurements, archived data sets, and refined data products such as ephemerides and their associated covariances. These data and services are accessed via a RESTful application programming interface (API)[2].

At present, LeoLabs' platform includes access to the following data through its API:

- *Raw measurements* - Calibrated range and range-rate measurements on RSOs, including correction values and uncertainty estimates;
- *Planned passes* - Data about planned instrument observations of RSOs, along with detection probability;
- *Statistics* - Statistics on the tracking of a given RSO, such as how many times the object has been observed;

[2] `https://platform.leolabs.space`

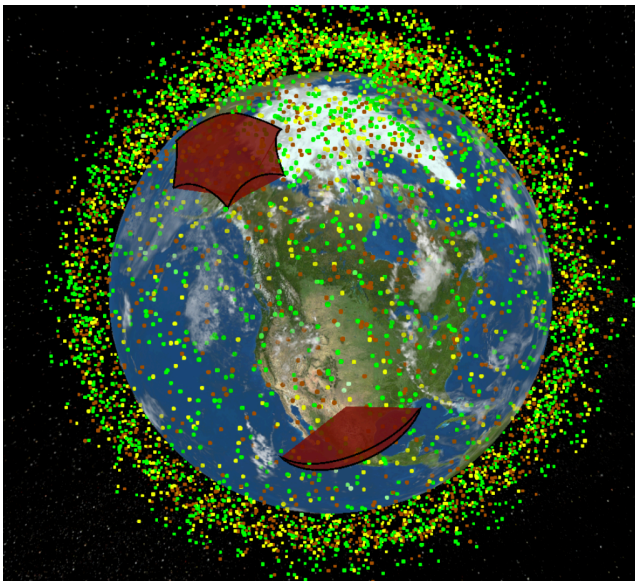

Figure 6: The FOVs of LeoLabs two radar sensors, along with a snapshot of objects tracked in LEO.

- *State vectors and ephemerides* - State vector (position and velocity) fitted to measurements, along with complete covariance, propagated to a user-specified time period;
- *TLEs* - TLEs on tracked objects;
- *Object prioritization* - The ability to request prioritization on a given object.

Fig. 7 shows statistics of LeoLabs' revisit rate over a typical 30-day period. Over this period, the radars tracked nearly 10,000 objects. LeoLabs is currently tracking most objects in the LEO portion of the public JSpOC catalog. More objects are tracked at PFISR because of its higher sensitivity. Most objects tracked by LeoLabs were tracked about once every 1-2 days. As the network expands over the next two years, we expect the revisit rate to be >4 times per day on most objects. High-interest objects (such as those named in a CDM) can be prioritized for tracking.

4. RADAR DATA PROCESSING AND VALIDATION

4.1. BIASES AND RESIDUALS

In order to consistently maintain high quality data products, it is important that LeoLabs' sensors deliver calibrated and verifiable raw measurements, as well as accurate uncertainty estimates. To accomplish this, LeoLabs makes use of data products provided by the International Laser Ranging Service (ILRS) [12]. The ILRS provides precise ranging on a

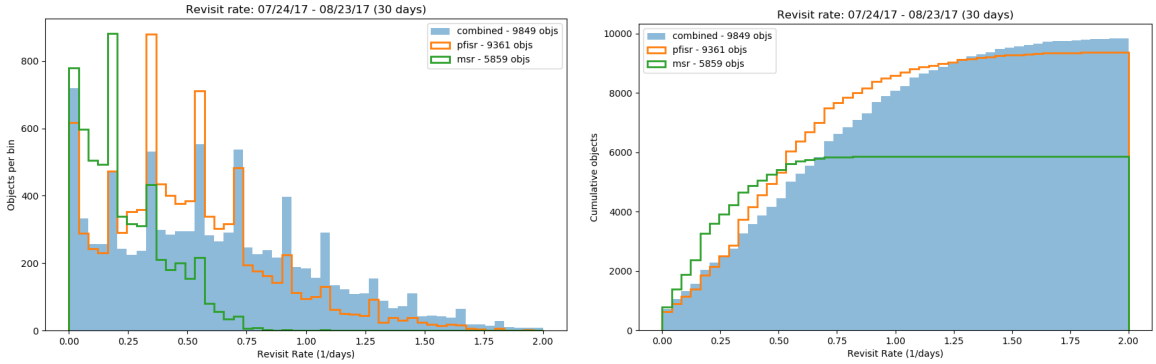

Figure 7: (Left) Histogram of revisit rates over a 30 day period and (right) corresponding cumulative distribution.

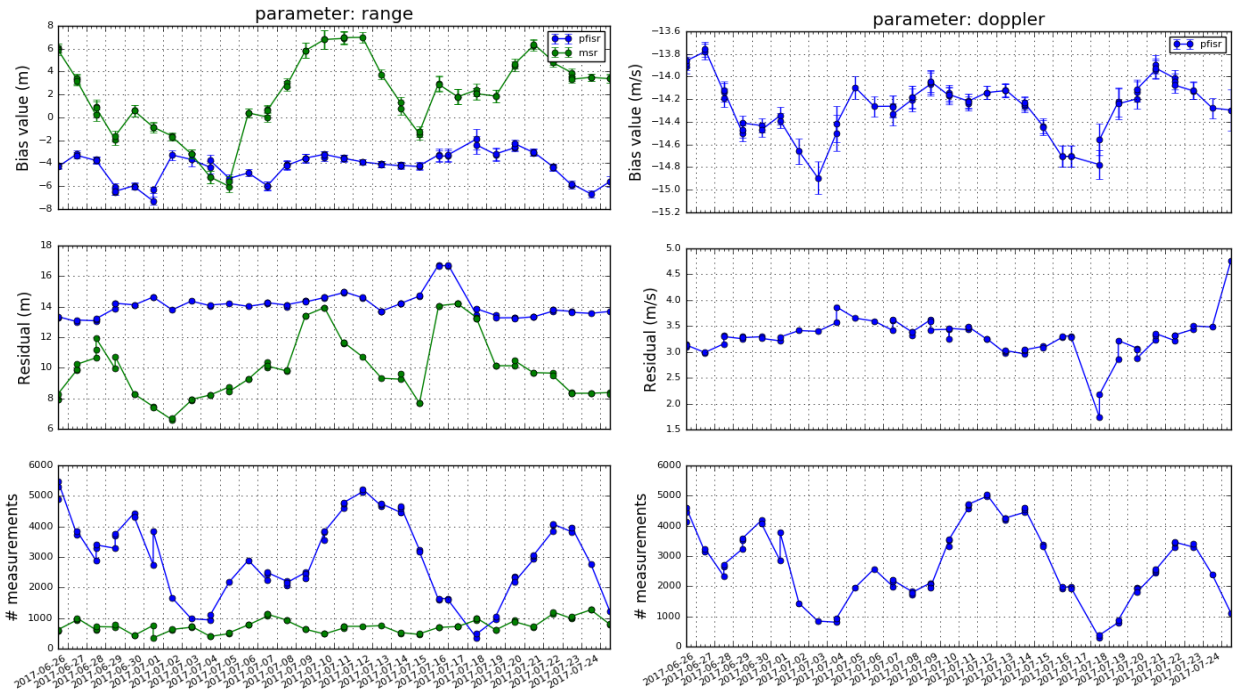

Figure 8: Biases with bias uncertainties (top), residuals (middle), and number of measurements used (bottom) for range (left) and doppler (right) for PFISR and MSR over approximately 1 month.

set of objects, as well as ephemeris predictions. LeoLabs regularly tracks these objects. After each pass, the range, doppler, and other measurements are compared to the ILRS truth data. These statistics are aggregated over all targets and a mean bias and residual are computed for each sensor several times per day.

Fig. 8 shows an example of the range biases over about a 1-month period in June/July 2017. Biases are $<$10 m for both systems and fluctuate by $\sim \pm 5$ m, likely due mainly to ionospheric variability. The errors on the biases are $<$1 m for both systems. The range residuals of the data (second row) are in the range 6-15 m for MSR, and 13-15 m for PFISR. All data provided through the LeoLabs API is corrected with the biases computed in real-time and available within minutes of collection.

4.2. EPHEMERIDES

The base state for a LeoLabs ephemeris begins with an OD accomplished via a BLS fit provisioned by the open source Orekit space dynamics library[3]. Fits begin by pulling recent data for an object from the LeoLabs measurement API. This data is culled to encompass at most the previous 7 transits before the bias-corrected range and range-rate measurements (along with their corresponding estimated uncertainties) are added to a BLS fitter. Successive fits may be attempted, rejecting outliers as necessary. Fitting terminates if the reduced χ^2 (e.g., see [14]) is less than or equal to 3, or fails to fall below 90% of the previous attempt's value. The epoch of the fit result is set to the time of the last measurement included in the fit, and uploaded to the LeoLabs API.

Fits and propagations performed by LeoLabs include the following effects and models:

- Detailed gravity provided by the JGM3 model [15], out to degree and order 42;
- Atmospheric drag provided by the DTM-2000 thermosphere model [2];
- Solar radiation pressure;
- Third body effects (Sun and Moon).

In addition to position and velocity vectors, the OD process also solves for c_d and c_r, the coefficients of drag and reflectivity relevant to the effects of atmospheric drag and solar radiation pressure. For both fits and propagations the spacecraft mass is set to 1 kilogram, and the body of the spacecraft is modeled as a sphere for the purposes of

[3] https://www.orekit.org

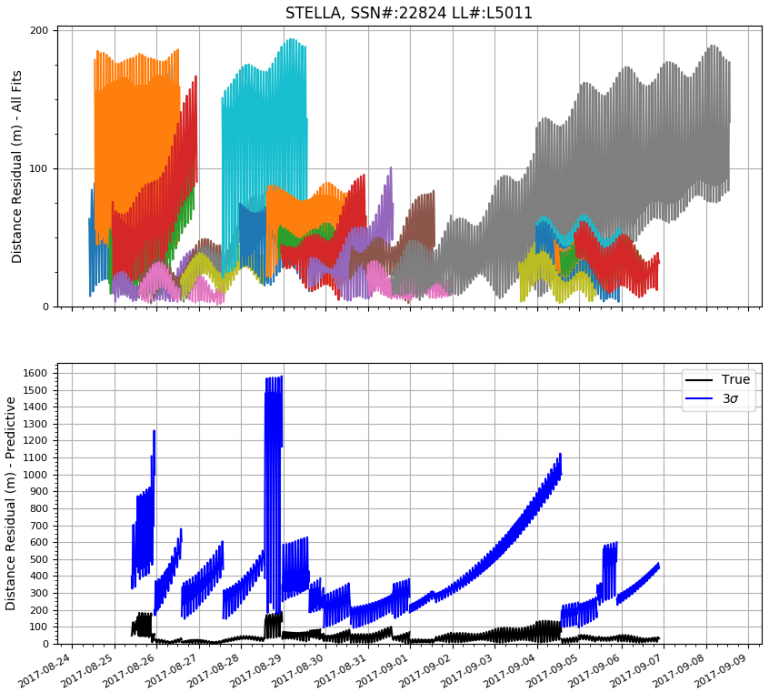

Figure 9: Comparison of LeoLabs OD to ILRS truth ephemeris. (Top) Distance residuals for all fits $\pm$24 hrs from fit epoch (except for the gray curve, which has been propagated forward 7 days). (Bottom) Predictive residuals (black) and 3σ uncertainties.

atmospheric drag and solar radiation pressure. While the aforementioned describes the nature of the LeoLabs OD system at the time of writing, this configuration will evolve to include different models and effects for performance and results optimization.

Any fitted state vector available in the API can be used as the base state for an ephemeris. Base states are propagated to the beginning of an indicated ephemeris window, where the state is captured at a user-specified timestep interval until the end of the window of interest. When finished, the resulting ephemeris is uploaded to the LeoLabs API, where it is retrievable by the user in JSON format.

An example of a comparison of LeoLabs OD to ILRS truth ephemeris [12] is shown in Fig. 9. After every pass over a LeoLabs radar sensor, a new OD is performed. This state vector is propagated $\pm$24 hours from fit epoch, and compared to the ILRS ephemeris to compute a residual. These comparisons are shown in the top panel of Fig. 9 for the Stella 24-cm sphere. One of the state-vector fits (gray) has been propagated 7-days forward. The bottom panel shows the "predictive residual" - i.e., the most recent state is propagated to the given time, such that the comparison is causal and is a measure of the performance at any given time instant. Also shown is the 3σ uncertainty (blue). For this RSO, the residuals are typically in the low tens of meters and well-bounded by the 3σ uncertainties.

4.3. COVARIANCE

At the end of a successful fit, the full 8x8 covariance matrix (representing position and velocity as well as the drag and reflectivity coefficients) can be requested from the BLS estimator. The time evolution (propagation) of the covariance matrix is achieved through the use of an unscented transform (e.g., [7]). Using this method the full 8x8 covariance is sampled using only 16 state vectors, avoiding the cumbersome calculation time required for a Monte-Carlo approach. These 16, 8-component vectors are propagated as individual orbits to any time of interest, where they provide all the information necessary to reconstitute a time-evolved covariance for the object in question. The methodology has been validated using a full Monte-Carlo approach for several cases (see Fig. 10).

Fitter-derived position covariance matrices are found to be optimistic. This effect is compensated for by the introduction of a scaling factor, which is computed in the following manner:

1. For a number of fits with truth data (e.g. ILRS targets), consider the state at fit epoch time and calculate the eigenvectors of each covariance matrix. Use these to represent an error vector describing the difference between the truth and estimated orbits in the eigenvector basis.
2. Assemble a dataset of normalized distances by dividing each vector component of the difference in the eigenvector basis with the associated eigenvalue. Do this for each fit.
3. Reject outliers and take the standard deviation of this dataset. This value is a covariance matrix scaling factor (see Fig. 11).
4. Recompute this scaling factor at a number of times between +/-1 day from fit epoch time (see Fig. 12). Fit a line to this dataset, and take the fit value at epoch time to be the covariance scaling factor used in analyses.

The error vector is represented in the covariance eigenspace rather than a more intuitive orbital frame such as RIC in order to ensure that the covariance ellipsoid is always sampled along physically meaningful directions.

To assess the validity of the covariance, the square of the Mahalanobis distance [9]

$$d^2 = \vec{x}^T C^{-1} \vec{x} \tag{4}$$

is calculated at fit epoch time for a number of states with covariance C and error vector $\vec{x}$. The distribution of d^2 values from both scaled and un-scaled covariances is compared against the expected χ^2-squared distribution. To account for propagation effects, a subset of states are propagated 7 days from fit epoch, and the relevant truth data is used to compute new d^2 squared values. As shown in Fig. 13, values of d^2 from the scaled covariance are seen to be in much better agreement with the expected χ^2-squared distribution than their unscaled counterparts. Scaling factors are determined in an automated fashion to ensure realistic propagated covariance.

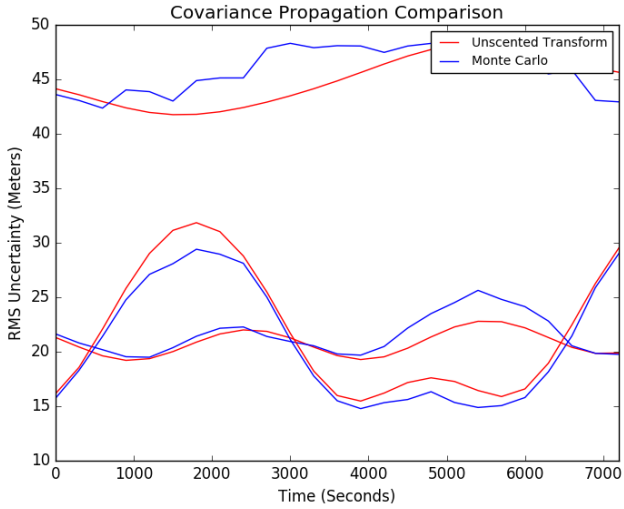

Figure 10: Comparison of RMS uncertainty derived from Monte-Carlo and unscented-transform covariance-propagation methods. In the former, 1000 samples are chosen at random based on a multivariate normal distribution with the specified covariance. In the latter, 16 sample points are selected using the unscented-transform algorithm. In both cases the covariance for a later time is calculated based on the distribution that results after the propagation of these sample points. Several states are inspected over the course of a 2-hour window occurring 1 day from fit epoch.

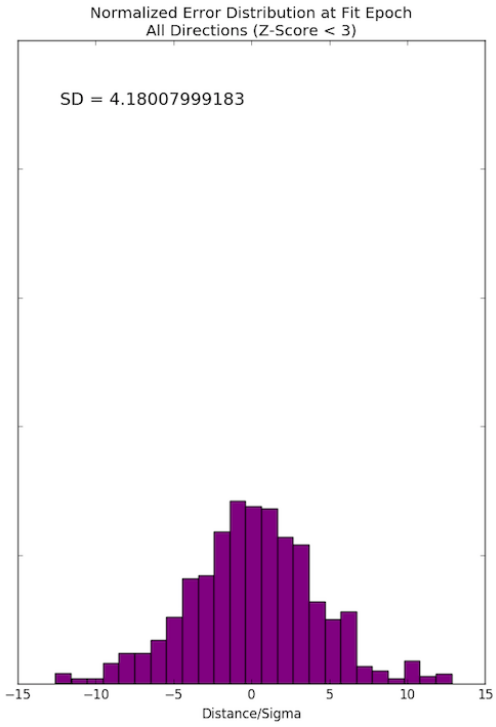

Figure 11: Distribution arising from the aggregate of normalized distances (distance divided by sigma) taken in each of the covariance eigenspace directions for a set of fits. The standard deviation of this distribution is the covariance scaling at $t = 0$.

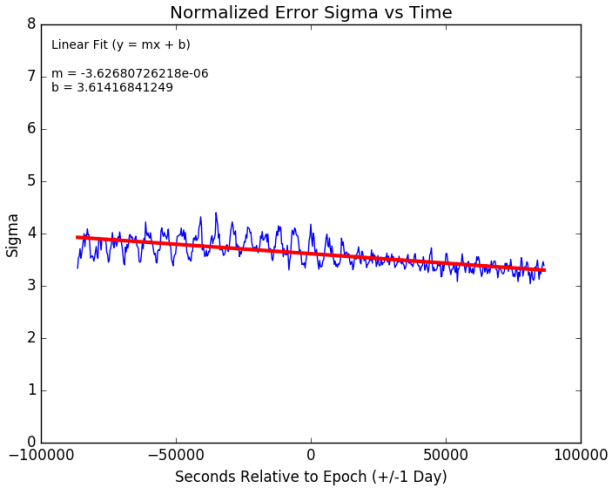

Figure 12: Linear fit to the covariance scaling factor computed at times between +/-1 day of fit epoch. The value from the fit at $t = 0$ is the scaling factor used in analyses.

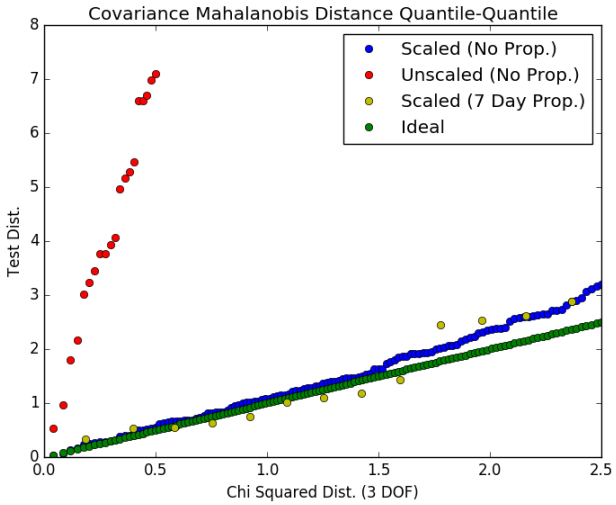

Figure 13: Quantile-quantile plot showing values of d^2 from the unscaled covariance (red) and the scaled covariance (green), compared with a line describing the expected χ^2-squared distribution (green). Yellow points represent the distribution of d^2 values from a subset of states that have been propagated 7 days.

4.4. COMPARISON BETWEEN RADAR AND SATELLITE DATA

Planet's large fleet of GPS-equipped satellites provides another way of independently validating radar data collected by the LeoLabs radar network. The Dove cubesats are exposed to high and varying drag forces due to various attitude maneuvers, and actively use GPS for OD purposes. The Doves are therefore a suitable test case for validating ranging. To evaluate individual measurements, GPS measurements collected during a tight interval centered around a measurement epoch are used to fit an orbit, which is extremely accurate and is considered to be the truth at the exact time of the measurement. It should be noted that the short-period fit is not suitable for long-period predictions and is only used for validating ranging measurements.

Approximately 1500 measurements for each LeoLabs radar are randomly sampled between May 28 and August 11, 2017. Fig. 14 shows the residuals for ranging measurements from MSR and PFISR. After filtering for outliers (which likely stem from mis-identification of the many Planet satellites and account for 0.4% to 7.9% of the measurements, respectively) the recovered standard deviations are consistent with those shown in Sec. 4 after accounting for the short-period GPS fitting uncertainty. The ranging standard deviations including GPS fitting uncertainty for MSR and PFISR are 18 m and 28 m, respectively. Doppler radar measurements including GPS fitting uncertainty from PFISR have a filtered standard deviation of about 11 m/s.

4.5. PROBABILITY OF COLLISION

In Sec. 5 we will present an analysis of several conjunctions, which includes calculation of collision probability, P_c. Here we summarize the approach used for this calculation.

In a three-dimensional space, P_c is expressed in the integral of the probability density function (PDF) over the volume of a cylinder – a secondary object passes through an error ellipsoid and sweeps a volume. This integral is assumed to be equivalent to a two-dimensional PDF over a circle on an encounter plane [1], which is defined in a following equation:

$$P_c = \frac{1}{2\pi\sigma_x\sigma_y}\int_{-R}^{R}\int_{-\sqrt{R^2-x^2}}^{\sqrt{R^2-x^2}} \exp\left[-\frac{1}{2}\left\{\left(\frac{x-x_m}{\sigma_x}\right)^2+\left(\frac{y-y_m}{\sigma_y}\right)^2\right\}\right] dydx, \tag{5}$$

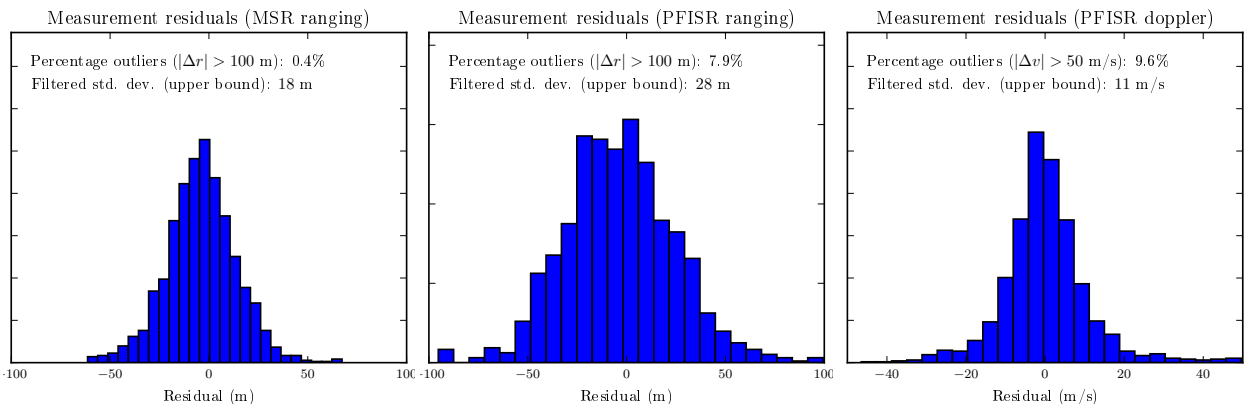

Figure 14: Residuals of raw radar measurements against GPS-derived Planet orbits. Histograms are normalized.

where (x_m, y_m), (σ_x, σ_y), and R represent a projected miss distance, the corresponding position standard deviations, and the combined object radius (COR), respectively. These values are acquired through following steps:

1. Define an encounter coordinate frame with respect to the primary object, and then transform the relative position vector and a combined covariance centered on the primary object to encounter frame representations.
2. Define the encounter plane, which reduces the 3-dimensional space to a 2-dimensional space.
3. Introduce an eigenspace to diagonalize the covariance for computing probability on the encounter plane.

In this research, we chose Alfano's method to compute the integration. This method converts the two-dimensional integration into a one-dimensional integral by introducing the error function, and then approximates the two-dimensional integral with a series of combined error functions and exponential terms [6]. For these examples we use the values in the final CDM before TCA as the closest approximation to "truth" available. Future efforts may include analyzing CDMs for which high-precision ephemeris are available on both objects.

5. CONJUNCTION CASE STUDIES

Multiple conjunctions between Doves and non-Dove secondaries are analyzed in this section. Each conjunction scenario is analyzed using a combination of JSpOC states (provided in the CDM), Planet data (for the primary satellite), and LeoLabs data (for both RSOs, but generally used only for the secondary object).

5.1. CASE A: SMALL DEBRIS CONJUNCTION

The first case studied involves the Flock 1c-4 (SSN 40031) primary satellite and a piece of small debris (SSN 34687), estimated to have an RCS of $\sim$0.03 m^2 from LeoLabs data (with other databases[4] reporting considerably smaller values, $\sim$0.005 m^2). The TCA for this conjunction was approximately 2017-06-11T13:12:48.5 UTC. The probability of collision (P_c) was low for this event (less than 10^{-9}) but the miss distance was only a few hundred meters.

Note that Planet no longer acquires GPS data from Flock 1c-4 since it no longer takes X-band passes - it belongs to a flock launched in 2014 and subsequent flocks have substantially surpassed it in image quality making it not worth taking X-band passes over newer satellites. Planet does however still routinely ranges the satellite on UHF and Flock 1c-4's ephemeris is based on this ranging data.

Fig. 15 shows an analysis based on LeoLabs data for this conjunction. For each new measurement on either the primary or secondary, the conjunction is re-analyzed. As part of this analysis, the primary and secondary states were propagated and interpolated around the TCA, and a new TCA, miss distance, and P_c were computed. Fig. 15a shows the miss distance with 1σ errors as a function of time. A dashed line shows the approximate miss distance of the final CDM. The miss distance estimated from LeoLabs data settles around the final expected value about 4 days prior to TCA. Note that the analysis continues after TCA, with the errorbars dropping dramatically and showing consistency with the LeoLabs solution. Fig. 15b shows the TCA evolution with time. The final TCA is within 0.05 seconds of the final CDM TCA, and again shows consistency within about 4 days of TCA. Fig. 15c shows the collision probability derived from

[4] http://n2yo.com

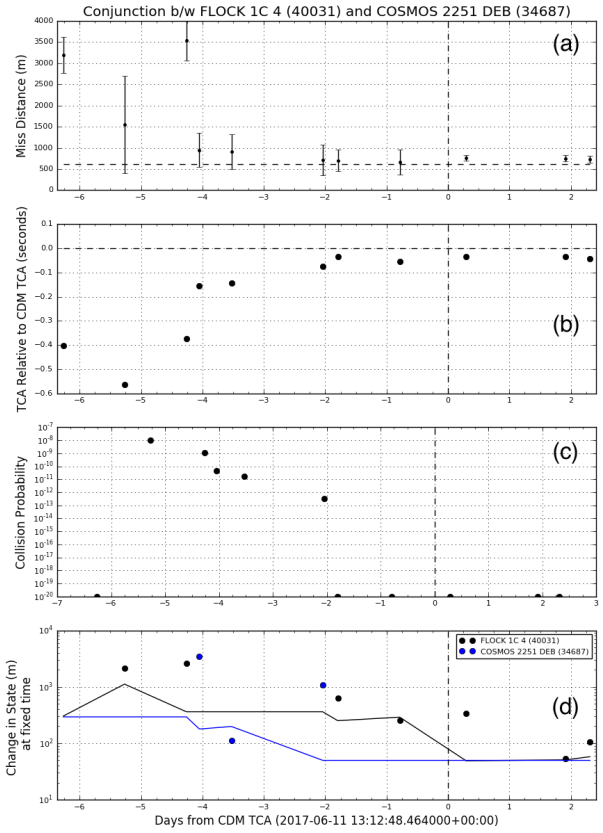

Figure 15: Conjunction analysis using LeoLabs data for the primary and secondary object. Panels show: (a) miss distance with 1σ errorbars as a function of time, with dashed lines displaying final CDM values; (b) estimates of the TCA relative to the final CDM TCA; (c) resulting probability of collision; (d) change in the primary and secondary state estimates at a fixed time close to TCA (points), along with the RMS errors on the states (solid lines).

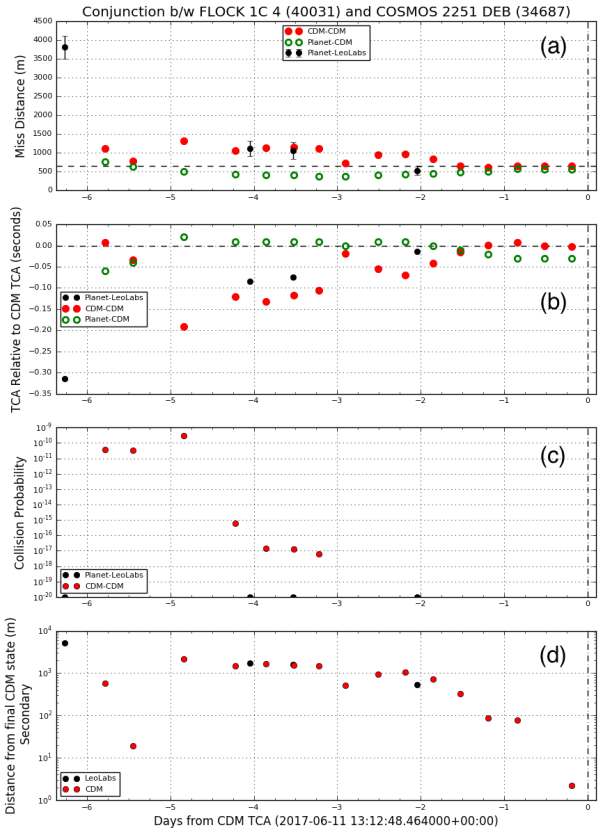

Figure 16: Conjunction analysis combining LeoLabs data on the secondary with Planet data on the primary. Panels show: (a) miss distances a function of time using CDM values (red points), using the Planet state for the primary with CDM secondary states (green), and using the Planet state for the primary and LeoLabs data for the secondary (black with errorbars); (b) estimates of the TCA relative to the final CDM TCA; (c) probability of collision from the CDMs (red) and from the Planet-LeoLabs data (black); and (d) distance between the secondary state estimates and the final CDM secondary state. Note that for panel (c) probabilities less than 10^{-20} have been assigned a value of 10^{-20}.

the LeoLabs state estimates on the primary and secondary. For this calculation, the probability was estimated using the method described in Sec. 4.5. P_c peaks at 10^{-8} about 5 days before TCA and drops from there to negligible values within 2 days of TCA. Fig. 15d shows the change in the states for the primary (black) and secondary object (blue) at a fixed time close to TCA, along with the estimated root-mean-square (RMS) error (solid lines) after propagation. The state estimates on both objects evolve consistently with variations of a few hundred meters up to a km in the days leading up to TCA. The RMS errors are a few hundred meters for the primary and less than a hundred meters for the secondary; these tight uncertainties drive the small errorbars on the miss distances and the small collision probabilities.

Fig. 16 shows the results of combining the LeoLabs data on the secondary with Planet data on the primary, and compared with data from the CDM. Panel (a) shows the miss distance provided by the CDM (red), computed using the Planet state on the primary and the CDM state on the secondary (green), and computed using the Planet state on the primary and the LeoLabs state on the secondary (black, with errorbars). Note that the Planet states used here were derived from a post analysis of ranging and/or GPS data. Panel (b) again shows the difference between the estimated

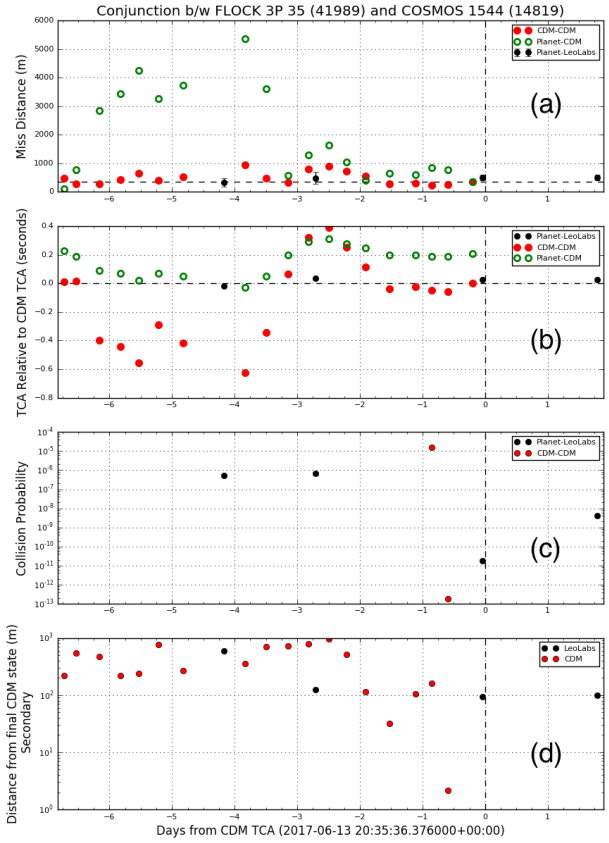

Figure 17: Same as Fig. 16 for Case B (see text for details).

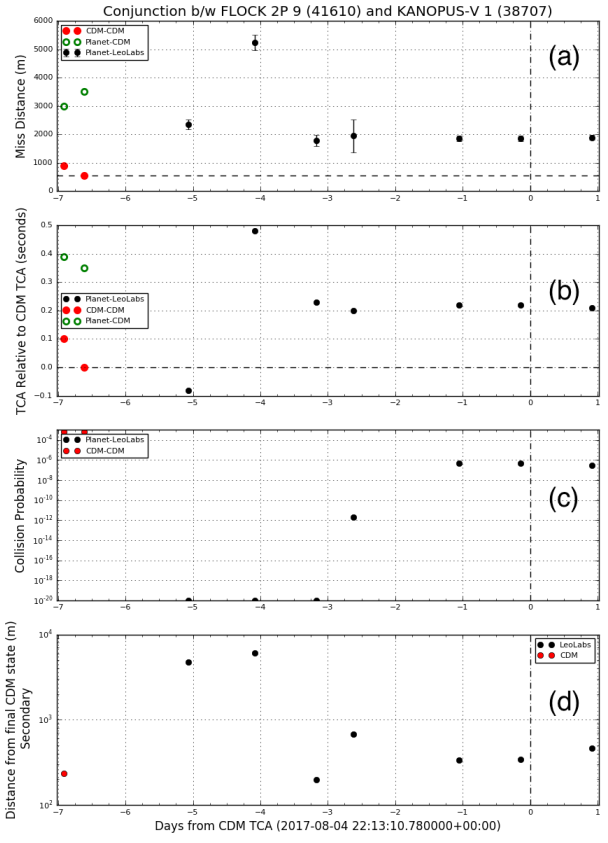

Figure 18: Same as Fig. 16 for Case C (see text for details).

TCA and the final CDM TCA. All three solutions show consistency in the days leading up to TCA, with the final miss distances within 100 meters of each other, and the final TCAs within 0.05 seconds of each other. Similarly, the P_c shown in panel (c) shows negligible values for both the CDM and the Planet-LeoLabs solution within 4 days of TCA.

Fig. 16d shows the distance between the final CDM secondary state and the secondary state vectors estimated by either the CDM (red) or LeoLabs (black). The secondary state of the CDM begins to settle to its final value about 2 days before TCA. The final LeoLabs solution is within 600 meters of the final CDM solution approximately 2 days prior to TCA. These solutions are close enough to drive consistent results within 2 days of TCA.

This case study demonstrates the utility of LeoLabs data for conjunctions with small debris. Solutions derived from LeoLabs data are consistent with CDM solutions and provide additional data leading up to TCA. By fusing conjunction estimates from two independent solutions, additional confidence can be gained with respect to predicting the evolution of conjunctions.

5.2. CASE B: CONJUNCTION WITH A LARGE SATELLITE

The second case studied involves the Flock 3p-35 (SSN 41989) primary satellite and a large satellite (SSN 14819). The TCA for this conjunction was approximately 2017-06-13T20:35:36.4 UTC. P_c was significant for this event, reaching above 10^{-5}, and the miss distance was only a few hundred meters.

Fig. 17 shows the results of combining Planet data on the primary and LeoLabs data on the secondary. Again, the three solutions (CDM-CDM, Planet-CDM, and LeoLabs-CDM) show consistency within 1-2 days of TCA, agreeing within 100 meters in miss distance and 0.2 seconds in TCA. The solution using the LeoLabs data on the secondary shows consistency with the final CDM approximately 4 days prior to TCA. The LeoLabs miss distance evolves by only about 100 meters over this period, and the TCA evolves by less than 0.05 seconds. The P_c (panel (c)) shows consistency 3 and 4 days prior to TCA, then drops considerably leading up to TCA. The LeoLabs secondary states (panel (d)) are

consistent within 3 days of TCA and agree with the final CDM secondary states within ∼100 meters. The LeoLabs solutions reach this level approximately 1 day before the CDM values. This case study again demonstrates the utility of adding independent data to a conjunction of significant risk, giving additional confidence in the conclusions derived from the conjunction analysis.

5.3. CASE C: CONJUNCTION WITH A SMALL SATELLITE

The final case, shown in Fig. 18, involves a conjunction between the Flock 2P-9 (SSN 41610) satellite and a small remote sensing satellite. This example illustrates the utility of using independent datasets when CDMs are not provided. In this case, two CDMs were received ∼6-7 days prior to TCA with very significant collision probabilities ($> 10^{-4}$) and miss distances of 500-1000 meters. However, no CDMs were received after this time, presumably because the conjunction fell below the threshold for warning. In this case, however, it would likely be of interest for an operator to continue monitoring the conjunction evolution. In this example, we demonstrate this capability using LeoLabs' independent data.

Here, the LeoLabs data initially shows a negligible P_c and large miss distance, but the estimates of the secondary state at TCA evolve and within ∼1 day of TCA P_c is $\sim 10^{-6}$ with a miss distance of about 1800 m. The TCA moves by less than 0.05 seconds within ∼3-4 days of TCA, and the secondary state estimated from the LeoLabs data evolves by only a few hundred meters during this time period. In the end, the LeoLabs secondary state is within a few hundred meters of the CDM value (estimated over 6 days earlier) but the miss distance and TCA are considerably different (over 1 km and 0.2 seconds, respectively).

In this case, the additional independent data provides the operator the ability to assess the collision risk despite not receiving additional CDMs. The consistency of the LeoLabs solutions, and the consistent evolution of miss distance and P_c, would allow the operator to confidently conclude that a conjunction-avoidance maneuver was unnecessary in this case.

6. SUMMARY AND FUTURE WORK

This study has demonstrated the utility of external data sources for providing additional insights into conjunctions. An operational workflow has been proposed for commercial satellite operators and commercial orbit-data providers to provide timely and accurate information on predicted conjunction events. This workflow is particularly applicable to operators that require automated machine-to-machine interfaces for rapid data access and automated decision making, which is critical for large constellations.

Commercial data provided by LeoLabs was compared to on-board GPS data from Planet as well as ILRS data and shown to be reliable, accurate, and timely. A set of example conjunctions was selected and for each of these miss distance, TCA, and probability of collision were calculated by combining LeoLabs and Planet data. The results were compared to the corresponding values provided in the CDMs. Ephemerides generated from LeoLabs data provide solutions and insights which are consistent with those provided in CDMs. With the additional data products, Planet can gain additional confidence in their interpretations of conjunction risks and can continue to monitor conjunctions for which additional CDMs are not available. In particular, Planet is able to utilize LeoLabs data to refine knowledge on secondary objects. This data ingestion can be used to reduce uncertainties, increase confidence in maneuver-related decisions, and reduce the number of false positives.

As commercial-sensor capabilities increase, so too will the quality and number of data products. LeoLabs' global network of radars, when completed, will provide multiple revisits per day on objects in LEO allowing for frequent state and conjunction updates. Sensitivity to smaller debris than is tracked today will provide insight into risks that are currently unknown.

Future work will focus on a statistical study of CDMs with combined LeoLabs and Planet-GPS data. Eventually, this may lead to an evaluation of CDMs provided purely by commercial data sources.

REFERENCES

[1] S. Alfano. Review of conjunction probability methods for short-term encounters. 127:719–746, 01 2007.

[2] S. Bruinsma, G. Thuillier, and F. Barlier. The DTM-2000 empirical thermosphere model with new data assimilation and constraints at lower boundary: accuracy and properties. *Journal of Atmospheric and Solar-Terrestrial Physics*, 65:1053–1070, June 2003.

[3] C. Foster, H. Hallam, and J. Mason. Orbit Determination and Differential-Drag Control of Planet Labs Cubesat Constellations. In *AIAA/AAS Astrodynamics Specialist Conference*, number AAS 15-524, Vail, CO, August 2015.

[4] C. Foster, J. Mason, V. Vittaldev, L. Leung, V. Beukelaers, L. Stepan, and R. Zimmerman. Differential Drag Control Scheme for Large Constellation of Planet Satellites and on-Orbit Results. In *9th International Workshop on Satellite Constellations and Formation Flying*, number IWSCFF 17-13, Boulder, CO, June 2017.

[5] A. Hawkins, J. Carrico, S. Motiwala, and C. MacLachlan. Flight Dynamics Operations and Collision Avoidance for the Skysat Imaging Constellation. In *9th International Workshop on Satellite Constellations and Formation Flying*, number IWSCFF 17-05, Boulder, CO, June 2017.

[6] T. A. Jackson. Study of the risk of impact between a spacecraft and space debris. Master's thesis, Universitat Politcnica de Catalunya, 2013.

[7] S. J. Julier. The scaled unscented transformation. In *Proceedings of the 2002 American Control Conference*, November 2002.

[8] F. G. Lemoine, D. E. Smith, L. Kunz, R. Smith, E. C. Pavlis, N. K. Pavlis, S. M. Klosko, D. S. Chinn, M. H. Torrence, R. G. Williamson, C. M. Cox, K. E. Rachlin, Y. M. Wang, S. C. Kenyon, R. Salman, R. Trimmer, R. H. Rapp, and R. S. Nerem. The Development of the NASA GSFC and NIMA Joint Geopotential Model. In Jiro Segawa, Hiromi Fujimoto, and Shuhei Okubo, editors, *Gravity, Geoid and Marine Geodesy: International Symposium No. 117 Tokyo, Japan, September 30 – October 5, 1996*, pages 461–469. Springer Berlin Heidelberg, Berlin, Heidelberg, 1997.

[9] P. C. Mahalanobis. On the generalised distance in statistics. In *Proceedings National Institute of Science, India*, volume 2, pages 49–55, April 1936.

[10] M. Nicolls. Space Debris Measurements using the Advanced Modular Incoherent Scatter Radar. In *Advanced Maui Optical and Space Surveillance Technologies Conference*, September 2015.

[11] D. Oltrogge, P. North, and M. Nicolls. Multi-phenomenology Observation Network Evaluation Tool (MONET). In *Advanced Maui Optical and Space Surveillance Technologies Conference*, September 2014.

[12] M. R. Pearlman, J. J. Degnan, and J. M. Bosworth. The International Laser Ranging Service. *Advances in Space Research*, 30:135–143, July 2002.

[13] J. M. Picone, A. E. Hedin, D. P. Drob, and A. C. Aikin. NRLMSISE-00 empirical model of the atmosphere: Statistical comparisons and scientific issues. *Journal of Geophysical Research (Space Physics)*, 107:1468, December 2002.

[14] W. H. Press, S. A. Teukolsky, W. T. Vetterling, and B. P. Flannery. *Numerical recipes in C. The art of scientific computing*. 1992.

[15] B. D. Tapley, M. M. Watkins, J. C. Ries, G. W. Davis, R. J. Eanes, S. R. Poole, H. J. Rim, B. E. Schutz, C. K. Shum, R. S. Nerem, F. J. Lerch, J. A. Marshall, S. M. Klosko, N. K. Pavlis, and R. G. Williamson. The Joint Gravity Model 3. *Journal of Geophysical Research*, 101:28, December 1996.